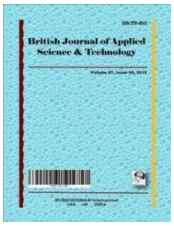

British Journal of Applied Science & Technology
15(2): 1-7, 2016, Article no.BJAST.24678
ISSN: 2231-0843, NLM ID: 101664541

SCIENCEDOMAIN *international*
www.sciencedomain.org

Hybrid Lateral Multi-junction Solar Cell Using Nonpolar $In_xGa_{(1-x)}N$ Material

Manoj Thosar[1*], R. K. Khanna[2] and Ashwini Joshi Thosar[3]

[1]Department of Physics, Vivekananda Institute of Technology-East, VIT Campus, Jaipur, India.
[2]Department of Physics, Vivekananda Global University, VIT Campus, Jaipur, India.
[3]Department of Electrical Engineering, Poornima University, Jaipur, India.

Authors' contributions

This work was carried out in collaboration between all authors. Author MT designed the study, performed the simulation and wrote the first draft of the manuscript. Author RKK supervised the research. Author AJT managed literature searches and did the final proof reading. All authors read and approved the final manuscript.

Article Information

DOI: 10.9734/BJAST/2016/24678
Editor(s):
(1) Essam E. Khalil, Professor of Energy, Cairo University, Cairo, Egypt.
Reviewers:
(1) Ioana Stanciu, University of Bucharest, Romania.
(2) Anonymous, Indiana University, USA.
(3) S. B. Ota, Institute of Physics, Sachivalaya Marg, Bhubaneswar, India.
Complete Peer review History: http://sciencedomain.org/review-history/13707

Original Research Article

Received 29th January 2016
Accepted 1st March 2016
Published 15th March 2016

ABSTRACT

The efficiency of nonpolar $In_xGa_{(1-x)}N$ material based hybrid lateral multi-junction solar cells was simulated using finite element approach. In this work we have used p-i-n and p-n structures for designing the sub-cells of hybrid lateral multi-junction solar cells. We have optimized both the sub-cell structures separately at different values of indium composition (x) for maximum efficiency. We have proposed fourteen sub-cells for our hybrid lateral multi-junction solar cell device through which it absorbs solar spectrum from 0.3 to 1.7 μm wavelength range. Results of simulation are presented here, which predict 37.08% average efficiency for lateral multi-junction solar cell based on p-i-n sub-cells while 40.21% average efficiency for lateral multi-junction solar cell based on p-n sub-cells. But the proper hybrid combination of p-i-n and p-n sub-cells provided 41.5% average efficiency.

Keywords: Vertical Multi-Junction (VMJ) solar cell; Lateral Multi-Junction (LMJ) solar cell; Nonpolar $In_xGa_{(1-x)}N$ material; p-i-n solar cell and optical beam splitter.

**Corresponding author: E-mail: labhesh9@gmail.com;*

1. INTRODUCTION

A multi-junction solar cell facilitates us to absorb complete solar spectrum from ultra-violet to infra-red region [1-4]. It contains multiple p-n junctions of different materials. These p-n junctions are called sub-cells. These sub-cells are connected in such a way, that they can absorb maximum range of solar spectrum and convert it into electrical power [5-7]. In VMJ solar cells, spectrum splitting is performed by the sub-cells as shown in Fig. 1.

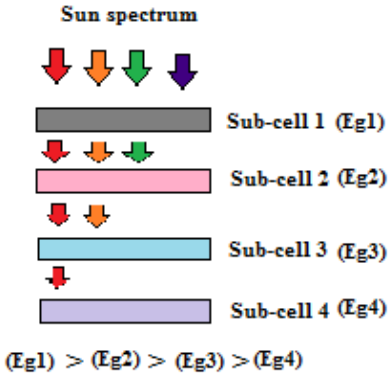

Fig. 1. Basic arrangement of sub-cells in VMJ solar cell

In VMJ solar cells, the sub-cells are arranged vertically one on one with ascending order of their energy band gap. When solar radiations are incident on the top surface of the solar cell, every sub-cell absorbs the radiation of energy greater than energy band gap and passes the remaining radiations to the next sub-cell just below it [6,8]. In such a way, maximum radiations are absorbed by VMJ solar cell. VMJ solar cells are grown monolithically [9,10]. In general VMJ solar cells are more expensive compare to single junction solar cells due to the expensive fabrication steps involved in growing layers of materials with lattice mismatch. Moreover, strain and interface defects significantly affect the performance of VMJ solar cells [9,11]. The highest 40.7% efficiency has been achieved by using this structure [9,12].

The LMJ solar cell works as an important solution for the problems associated with VMJ solar cell. In LMJ solar cells, the optical beam splitter is used for splitting the solar spectrum into the desired bandwidth [13-15]. The basic arrangements of sub-cells in LMJ solar cell is shown in Fig. 2.

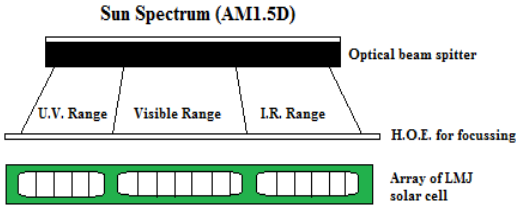

Fig. 2. Basic arrangements of sub-cells in LMJ solar cell

The sub-cells of LMJ solar cell are connected externally, therefore it provides greater flexibility in terms of interconnections of sub-cells and material choice issues and yield higher efficiency [16,17]. Further improvement in LMJ solar cell will be possible by utilizing the flexibility of choosing the sub-cells independently. In present work we have optimized the sub-cells of p-i-n and p-n structures. Results show that proper combination of these sub-cells offer a chance to achieve better efficient Hybrid Lateral Multi-Junction (HLMJ) solar cell.

Nonpolar $In_xGa_{(1-x)}N$ alloy is the most suitable material for photovoltaic applications. This alloy has direct band gap property at entire energy band gap range, which makes this material suitable for generating and absorbing light [18], [19]. $In_xGa_{(1-x)}N$ material can absorb solar spectrum from 0.3 to 1.7 μm wavelength by changing indium composition (x) from 0 to 1 [18], [19]. Therefore nonpolar $In_xGa_{(1-x)}N$ material is capable of absorbing more than 80% radiations of AM1.5D spectrum of the sun.

2. RELATIONS AND PARAMETERS OF $In_xGa_{(1-x)}N$ MATERIAL USED IN SIMULATION

The energy band gap $E_{g(In_xGa_{(1-x)}N)}$, Relative permittivity $\varepsilon_{(In_xGa_{(1-x)}N)}$, Electron affinity $\chi_{(In_xGa_{(1-x)}N)}$, Absorption coefficient α(λ), Refractive index $n_{(In_xGa_{(1-x)}N)}$, Effective density of states in the conduction band $N_{C(In_xGa_{(1-x)}N)}$, Effective density of states in the valence band $N_{V(In_xGa_{(1-x)}N)}$, Electron mobility $\mu_{e(N)}$, Hole mobility $\mu_{h(N)}$ and Lattice constant $a_{(In_xGa_{(1-x)}N)}$ for $In_xGa_{(1-x)}N$ material at different indium composition (x) is calculated by using the relations from equation-1 to 10 and the required values of GaN and InN material parameters for simulation are listed in Table 1 [18-22].

Table 1. Parameters of GaN and InN used in simulation

Parameter (wurtzite structure)	GaN	InN
Carrier life time (ns) [21]	1	1
Energy band gap (eV) [21]	3.42	0.7
Bowing parameter (eV) [22]	1.43	1.43
Relative permittivity [21]	8.9	10.5
Electron affinity (eV) [21]	4.1	6
Refractive index [20]	2.65	2.9
Effective density of states in the conduction band (cm^{-3}) [21]	2×10^{17}	8×10^{18}
Effective density of states in the valence band (cm^{-3}) [21]	3×10^{17}	3×10^{17}
Maximum electron mobility ($cm^2eV^{-1}s^{-1}$) [21]	1000	1100
Maximum hole mobility ($cm^2eV^{-1}s^{-1}$) [21]	170	340
Minimum electron mobility ($cm^2eV^{-1}s^{-1}$) [21]	55	30
Minimum hole mobility ($cm^2eV^{-1}s^{-1}$) [21]	3	3
Lattice constant (Å) [20]	3.189	3.548
Electron saturation velocity (cm/sec.) [20]	2.5×10^7	2.5×10^7

$$E_{g(In_xGa_{(1-x)}N)} = xE_{g(InN)} + (1-x)E_{g(GaN)} - bx(1-x) \quad (1)$$

$$\varepsilon_{(In_xGa_{(1-x)}N)} = x\varepsilon_{(InN)} + (1-x)\varepsilon_{(GaN)} \quad (2)$$

$$\chi_{(In_xGa_{(1-x)}N)} = \chi_{(GaN)} + 0.7\left[3.42 - E_{g(In_xGa_{(1-x)}N)}\right] \quad (3)$$

$$\alpha(\lambda) = 2.2\times10^5\left[\left(\frac{1.24}{\lambda}\right) - E_{g(In_xGa_{(1-x)}N)}\right]^{\frac{1}{2}} \quad (4)$$

$$n_{(In_xGa_{(1-x)}N)} = xn_{(InN)} + (1-x)n_{(GaN)} - bx(1-x) \quad (5)$$

$$N_{C(In_xGa_{(1-x)}N)} = xN_{C(InN)} + (1-x)N_{C(GaN)} \quad (6)$$

$$N_{V(In_xGa_{(1-x)}N)} = xN_{V(InN)} + (1-x)N_{V(GaN)} \quad (7)$$

$$\mu_{e(N)} = \mu_{e(min)} + \left[\frac{\mu_{e(max)}-\mu_{e(min)}}{1+(\frac{N}{N_C})}\right] \quad (8)$$

$$\mu_{h(N)} = \mu_{h(min)} + \left[\frac{\mu_{h(max)}-\mu_{h(min)}}{1+(\frac{N}{N_V})}\right] \quad (9)$$

$$a_{(In_xGa_{(1-x)}N)} = xa_{(InN)} + (1-x)a_{(GaN)} \quad (10)$$

Where, $E_{g(InN)}$ and $E_{g(GaN)}$ are the energy band gap of InN and GaN material. 'b' is called the bowing parameter for $In_xGa_{(1-x)}N$ material. $\varepsilon_{(InN)}$ and $\varepsilon_{(GaN)}$ are the relative permittivity of InN and GaN material. $\chi_{(GaN)}$ is the electron affinity of GaN. $n_{(InN)}$ and $n_{(GaN)}$ are the refractive indies of InN and GaN respectively. $N_{C(InN)}$ and $N_{C(GaN)}$ are the effective density of states in the conduction band of InN and GaN material. $N_{V(InN)}$ and $N_{V(GaN)}$ are the effective density of states in the valence band of InN and GaN material. $\mu_{e(max)}$ and $\mu_{e(min)}$ are the maximum and minimum electron mobility in $In_xGa_{(1-x)}N$ material. $\mu_{h(max)}$ and $\mu_{h(min)}$ are the maximum and minimum hole mobility in $In_xGa_{(1-x)}N$ material. $a_{(InN)}$ and $a_{(GaN)}$ are the lattice constant of InN and GaN material respectively.

3. METHOD

The energy band gap of nonpolar $In_xGa_{(1-x)}N$ material has controlled by varying indium composition (*x*) from 0 to 1. This material can

Table 2. Optical and electrical parameters of $In_xGa_{(1-x)}N$ material at different indium composition (*x*)

Sub-cell number	Cutoff wavelength(λ_c) in μm	Required Indium composition (*x*)	Energy gap (Eg) in eV	Refractive index (n)	Absorption coefficient $\alpha(\lambda_c)$ in 10^5 cm^{-1}
1	0.4	0.08	3.10	2.56	1.48
2	0.5	0.24	2.48	2.45	1.15
3	0.6	0.37	2.06	2.40	0.98
4	0.7	0.45	1.77	2.40	0.81
5	0.8	0.55	1.55	2.42	0.69
6	0.9	0.63	1.37	2.47	0.65
7	1.0	0.69	1.24	2.51	0.55
8	1.1	0.74	1.12	2.56	0.54
9	1.2	0.79	1.03	2.61	0.48
10	1.3	0.83	0.95	2.65	0.44
11	1.4	0.87	0.88	2.70	0.43
12	1.5	0.91	0.82	2.75	0.41
13	1.6	0.95	0.77	2.82	0.37
14	1.7	0.98	0.72	2.86	0.35

absorb solar spectrum from 0.3 to 1.7 μm wavelength. In this work, we have divided above 1.4 μm wavelength absorption range into fourteen parts and accordingly find out the values of indium composition (*x*) for $In_xGa_{(1-x)}N$ material. All the required optical and electrical parameters of $In_xGa_{(1-x)}N$ material at different indium composition (*x*) are calculated and listed in Table 2.

We have started the simulation process with a p-$In_xGa_{(1-x)}N$/n-$In_xGa_{(1-x)}N$ solar cell structure by using PC1D (version 5.9) simulation software. Here we have considered that solar radiations of AM1.5D spectrum are entering from n-$In_xGa_{(1-x)}N$ region. We have used untextured upper surface with good quality passivation layer. We have optimized the thickness of n-$In_xGa_{(1-x)}N$ and p-$In_xGa_{(1-x)}N$ regions at different values of indium composition (*x*) for maximum efficiency. In the next step of simulation, an i-$In_xGa_{(1-x)}N$ layer has inserted between p-GaN and n-GaN region. After that we have changed the value of indium composition (*x*) in i-$In_xGa_{(1-x)}N$ layer and optimized the thickness of i- $In_xGa_{(1-x)}N$ layer for maximum efficiency.

4. RESULTS AND DISCUSSION

The carrier life time is the direct indicator of material quality [23]. Study of $In_xGa_{(1-x)}N$ material shows that the carrier lifetime for considerable quality of the material should be 1ns. For $In_xGa_{(1-x)}N$ material, as we increase the value of indium composition (x), the quality of the material is degraded. This reduction in quality of $In_xGa_{(1-x)}N$ material is due to the size difference between the indium and gallium atoms. This difference generates the lattice defects and also changes the internal polarization field. The devices fabricated by using nonpolar $In_xGa_{(1-x)}N$ material is free from the polarization effect, but exaggerated by the lattice defects like trapping centers and dislocation density [18,23-25]. It is well known that for good quality material, the p-n structure of solar cell is more efficient than p-i-n structure solar cell [21]. In this work we have considered 1ns lifetime of carriers for the $In_xGa_{(1-x)}N$ material. Here we have used the p-i-n hetrostructure for designing the sub-cells of LMJ solar cell. In this structure p and n regions are made by GaN material while i-layer is formed by using $In_xGa_{(1-x)}N$ material. We have got 100nm thick n-GaN and 400 nm thick p- GaN layer for designing the p-i-n hetrostructure sub-cells through the simulation. The thickness of n-GaN layer plays a vital role in device efficiency. Large thickness of n-GaN layer makes the device bulky and less transparent for light. But small thickness of n-GaN layer should be problematic in fabricating ohmic contacts for the device. An i-$In_xGa_{(1-x)}N$ layer is inserted between them and optimized the thickness of this layer for maximum efficiency. Fig. 3 shows the required thickness of i- $In_xGa_{(1-x)}N$ layer for maximum efficiency at different indium composition (*x*).

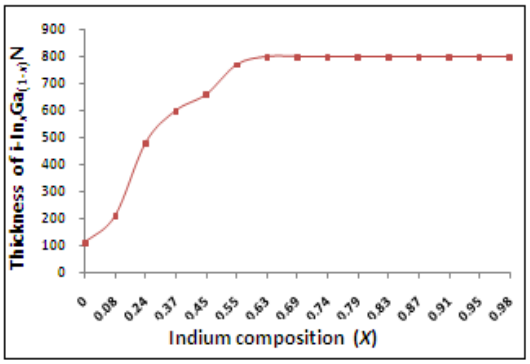

Fig. 3. Thickness of i- $In_xGa_{(1-x)}N$ layer for maximum efficiency

Graph indicates the saturation in thickness of i-$In_xGa_{(1-x)}N$ layer because of the saturation in absorption coefficient at higher values of indium composition (x). Further enhancement in efficiency is possible through the optimization of p-doping in i-$In_xGa_{(1-x)}N$ layer. The optimized value of p-doping for desired value of indium composition is shown in Fig. 4 and the maximum efficiency of p-i-n solar cell on optimized value of p-doping is shown in Fig. 5.

The maximum efficiency 53.53% has achieved at 1×10^{16} per cm^3 p-doping, 0.37 indium composition and 480 nm thickness of i-$In_xGa_{(1-x)}N$ layer with 10.7mA short circuit current and 2.598 volt open circuit voltage. Initially for small values of indium composition (x) in i-$In_xGa_{(1-x)}N$ layer, p-i-n structure sub-cells provides the better performance in comparison to p-n structure. The external efficiency of p-i-n and p-n sub-cells at different values of indium composition (x) is shown in Fig. 5.

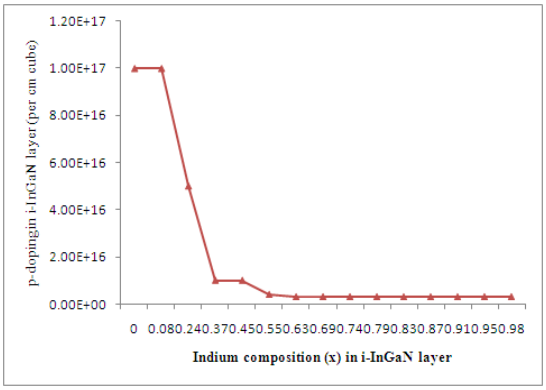

Fig. 4. Optimized p-doping in i-$In_xGa_{(1-x)}N$ layer

It is well known that the p-i-n hetrostructure solar cell provides better results with large energy difference between i- layer and n or p layer [23]. But the pattern of results are reversed after 45% of indium composition (x) in i-$In_xGa_{(1-x)}N$ layer. This change of pattern is due to the poor quality of $In_xGa_{(1-x)}N$ material at higher indium composition (x). The lattice mismatch generates the trapping centers at the interface of two layers. These trapping centers trap the photo carriers pass through it [23,26,27]. But the conduction band offset plays a vital role in degrading the performance of p-i-n hetrostructure sub-cells. This conduction band offset works as a barrier for those photo electrons which passes the n-GaN/i-$In_xGa_{(1-x)}N$ interface [26]. Finally one

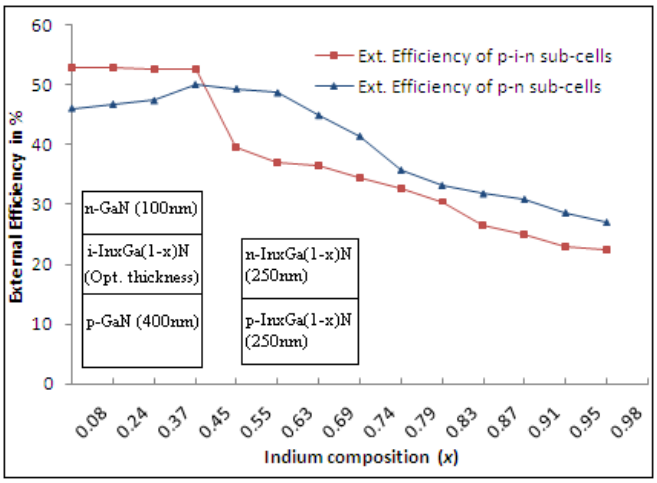

Fig. 5. The external efficiency of p-i-n and p-n sub-cells at different values of indium composition (x)

got better results for p-n sub-cells for higher values of indium composition (*x*) in sub-cells. Results shows that the performance of p-i-n sub-cells are better than p-n sub-cells up to 45% of indium composition and after that results are reversed. For designing HLMJ solar cell, it is suggested that p-i-n sub-cells can used up to 45% indium composition and remaining from p-n sub-cells for higher indium composition. The average efficiency of LMJ solar cell based on p-i-n sub-cells was 37.08% and 40.21% for p-n sub-cells while through the proposed model of HLMJ solar cell one can achieve the 41.5% average efficiency.

5. CONCLUSION

Results of simulation, study and proposed design of HLMJ solar cell indicates that the flexibility of choosing the sub-cells in LMJ solar cell improve the performance. The efficiency of LMJ solar cell with p-i-n sub-cells was 37.08%. This efficiency improved further by 8.44% using p-n sub-cells. But finally the use of proper combination of p-i-n and p-n sub-cells in the proposed HLMJ solar cell provided 41.5% efficiency. This efficiency is greater than 11.92% from LMJ solar cell using p-i-n sub-cells and 3.2% of using p-n sub-cells.

ACKNOWLEDGEMENTS

Authors are thankful to the management of Vivekananda Group of Institutions, Jaipur for providing facility for the work.

COMPETING INTERESTS

Authors have declared that no competing interests exist.

REFERENCES

1. Bhuiyan A, Sugita K, Hashimoto A, Yamamoto A. InGaN solar cells: Present state of the art and important challenges. IEEE J. Photovoltaics. 2012;2:276-293.
2. Tribus E, Namkoong G, Henderson W, Burnham S, Doolittle WA, Cheung M, Cartwright A. InN: A material with photovoltaic promise and challenges. J. Cryst. Growth. 2006;288:218-224.
3. Hamzaoui H, Bouazzi AS, Rezig B. Theoretical possibilities of InGaN tandem PV structure. Solar Energy Materials and Solar Cells. 2005;87:595-603.
4. Jani O, Honsberg C, Asghar A. Characteristics and analysis of InGaN photovoltaic devices. In Proceedings of the 31st IEEE Photovoltaic Specialists conference, Lake Buena Vista, Fla, USA. 2005;37-42.
5. Green Martin A, Ho-Baillie A. Forty three percent composite split-spectrum concentrator solar cell efficiency. Prog. Photovolt: Res. Appl. 2010;18:42-47.
6. Sachenko AV, Kulish MR, Sokolovskyi IO, Kostylyov VP. Lateral multijunction photovoltaic cells. Semiconductor Physics, Quantum Electronics & Optoelectronics. 2013;16:1-17.
7. Barnett A, Honsberg C, Kirkpatrick D. 50% efficient solar cell architecture and designs. IEEE 4th Word Conf. Photovoltaic Energy Conversion. 2006;2:2560-2564.
8. Caselli DA, Ning CZ. High-performance laterally-arranged multiple-bandgap solar cells using spetially composition-graded $Cd_XPb_{1-X}S$ nanowires on a single substrate: A design study. Optics Express. 2011;19:A686-A694.
9. Alam MK, Khan F, Imtiaz AM. Optimization of subcell interconnection for multijunction solar cells using switching power converters. IEEE Transaction on Sustainable Energy. 2012;4:340-349.
10. Imenes AG, Mills DR. Spectral beam splitting technology for increased conversion efficiency in solar concentrating system. Solar Energy Materials and Solar Cells. 2004;84:16-69.
11. Karp JH, Ford JE. Multiband solar concentrator using transmissive dichroic beam splitting. in Proc. SPIE. 2008;7043: 70430F-70430F-8.
12. King RR, Boca A, Hong W, Law D, Kinsey G, Fetzer C, Hadded M, Edmondson K, Yoon H, Pien P, Karem N. High efficiency multijunction photovoltaics for low cost solar electricity. in Proc. Ann. Meeting IEEE Lasers and Electro-Optics Society. 2008;2-3.
13. Bloss WH, Griesinger M, Reinhardt ER. Dispersive concentrating systems based on transmission phase holograms for solar applications. Appl. Opt. 1982;21:3739-3742.
14. Barnett A, Kirkpatrick D, Honsberg C, Moore D, Wanlass M, Emergy K, Schwartz R, Carlson D, Bowden S, Aiken D, Gray A, Kurtz S, Kazmerski L, Moriarty T, Steiner M, Gray J, Daveport T, Buelow R, Takacs L, Shatz N. Milestones towards 50% solar cell modules. Presented at the 22nd European Photovoltaics Solar Energy

Conference, Institute of Electrical and Electronics Engineers, Milan, Italy; 2007.
15. Ludman JE, Riccobono J, Semenova IV, Reinhand NO, Tai W, Li X, Syphres G, Rallis E, Sliker G, Martin J. The optimization of holographic system for solar power generation. Sol. Energy. 1997;60:1-9.
16. Lewis CR, Phillips WM, Shields VB, Stella PM. Multi-band high efficiency convertor (RAINBOW). In Proc. IECEC. 1997;401-406.
17. Lentine AL, Nielson GN, Okandan M, Sweatt WC, Cruzcampa JL, Gupta V. Optimal cell connections for improved shading, reliability and spectral performance of microsystem enabled photovoltaic (MEPV) modules. in Proc. 35th IEEE Photovoltaic Specialists Conf. (PVSC). 2010;3048-3054.
18. Fabien Chloe AM. Simulations, limitations and novel growth technology for InGaN-based solar cell. IEEE Journal of Photovoltaic. 2013;2156-3381.
DOI: 10.1109/JPHOTOV.2013.2292748
19. Levinshtein ME, Rumyantsev SL, Shu MS. Properties of advanced semiconductor materials. 2nd ed., John Wiley & Sons, New York, USA. 2001;234.
20. Aziz WJ, Ibrahim K. Simulation model for multi-junction InGaN solar cell. Int. J. Nanoelectronics and Materials. 2010;3:43-52.
21. Brown GF, Ager JW, Walukiewicz W, Wu J. Finite element simulations of compositionally graded InGaN solar cells. Solar Energy Materials and Solar Cells. 2010;94:478-483.
22. Wu J, Walukiewicz W, Yu KM. small band gap bowing in InGaN alloys. Applied Physics Letters. 2002;80:4741-4749.
23. Jeng Ming-Jer.: Simulation of nonpolar p-GaN/i-InGaN/n- GaN solar cells. International Journal of Photoenergy; 2012.
DOI: 10.1155/2012/910256
24. Bandic ZZ, Bridger PM, Piquette EC, McGill TC. Minority carrier diffusion length and life time in GaN. Applied Physics Letter. 1998;72:3166-3168.
25. Chen F, Cartwright AN, Lu H, Schaff WJ. Temperature dependence of carrier life times in InN. Phys. Status Solidi A. 2005;202:768-772.
26. Manoj Thosar, Khanna RK, Ashwini Joshi Thosar. Simulation of nonpolar p-GaN/i-$In_xGa_{(1-x)}N$/n-GaN solar cell for maximum efficiency. Presented at the International Conference on Recent cognizance in Wireless communication & Image Processing, Springer India, ICRCWIP; 2014.
DOI: 10.1007/978-81-322-2638-3
27. Kushwaha Aniruddha Singh, Mahala Pramila, Dhanavantri Chenna. Optimization of p-GaN/InGaN/n-GaN double heterojunction p-i-n solar cell for high efficiency: simulation approach. International Journal of Photoenergy; 2014. Article ID 819637.

Peer-review history:
The peer review history for this paper can be accessed here:
http://sciencedomain.org/review-history/13707